

Computer-Aided Diagnosis Scheme for Detection of Lacunar Infarcts on MR Images¹

Yoshikazu Uchiyama, Ryujiro Yokoyama, Hiromich Ando, Takahiko Asano, Hiroki Kato, Hiroyasu Yamakawa
Haruki Yamakawa, Takeshi Hara, Toru Iwama, Hiroaki Hoshi, Hiroshi Fujita

Rationale and Objectives. The detection and management of asymptomatic lacunar infarcts on magnetic resonance (MR) images are important tasks for radiologists to ensure the prevention of severe cerebral infarctions. However, accurate identification of the lacunar infarcts on MR images is a difficult task for the radiologists. Therefore the purpose of this study was to develop a computer-aided diagnosis scheme for the detection of lacunar infarcts to assist radiologists' interpretation as a "second opinion."

Materials and Methods. Our database comprised 1,143 T1- and 1,143 T2-weighted images obtained from 132 patients. The locations of the lacunar infarcts were determined by experienced neuroradiologists. We first segmented the cerebral region in a T1-weighted image by using a region growing technique for restricting the search area of lacunar infarcts. For identifying the initial lacunar infarcts candidates, a top-hat transform and multiple-phase binarization were then applied to the T2-weighted image within the segmented cerebral region. For eliminating the false positives (FPs), we determined 12 features—the locations x and y , signal intensity differences in the T1- and T2-weighted images, nodular components from a scale of 1 to 4, and nodular and linear components from a scale of 1 to 4. The nodular components and the linear components were obtained using a filter bank technique. The rule-based schemes and a support vector machine with 12 features were applied to the regions of the initial candidates for distinguishing between lacunar infarcts and FPs.

Results. Our computerized scheme was evaluated by using a holdout method. The sensitivity of the detection of lacunar infarcts was 96.8% (90/93) with 0.76 FP per image.

Conclusions. Our computerized scheme would be useful in assisting radiologists for identifying lacunar infarcts in MR images.

Key Words. Lacunar infarcts; magnetic resonance imaging; computer-aided diagnosis (CAD); filter bank; support vector machine.

© AUR, 2007

Cerebrovascular disease is the third major cause of death in Japan (1). Therefore, a health check system for cerebral and cerebrovascular diseases, which is named Brain Dock, is

widely performed in Japan. In this system, unruptured cerebral aneurysms and asymptomatic lacunar infarcts are often detected using magnetic resonance angiography (MRA) and magnetic resonance imaging (MRI). However, their accurate identification is difficult task for radiologists. Thus we have been developed computer-aided diagnosis (CAD) schemes in Brain Dock for the detection of cerebral and cerebrovascular diseases on brain magnetic resonance images (2–7) in order to assist radiologists' diagnosis as a "second opinion."

The detection of unruptured aneurysms in MRA studies is important because aneurysms rupture is the main cause of subarachnoid hemorrhage. However, it is difficult to detect small aneurysms in MRA studies because of the overlapping of aneurysms and adjacent vessels on maximum intensity projection image. Therefore several CAD schemes have

Acad Radiol 2007; 14:1554–1561

¹ From the Department of Intelligent Image Information, Graduate School of Medicine, Gifu University, Japan (Y.U., R.Y., T.H., H.F.); Department of Radiology, Graduate School of Medicine, Gifu University, Japan (T.A., H.K., H.H.); and Department of Neurosurgery, Graduate School of Medicine, Gifu University, Japan (H.Ya., T.I.); Department of Neurosurgery, Gifu Municipal Hospital, Japan (H.A.); Department of Emergency and Critical Care Medicine, Chuno-Kousei Hospital, Japan (H.Y.). Received December 25, 2006; accepted September 13, 2007. Supported in part by a grant for the "Knowledge Cluster Creation Project" from the Ministry of Education, Culture, Sports, Science, and Technology, Japan. **Address correspondence to:** Y.U. e-mail: uchiyama@fjt.info.gifu-u.ac.jp

© AUR, 2007

doi:10.1016/j.acra.2007.09.012

been reported for the detection of aneurysms in MRA studies (5,6,8–11). CAD schemes can determine the locations of the candidates for unruptured aneurysms by analyzing certain image features such as the size or shape of the candidate (5,8–11). Approximately 90%–95% of the aneurysms can be accurately detected using the current CAD schemes. An observer study for conducting the effect of a developed CAD scheme was also carried out (12). The results of this study indicated that the CAD improved the performance of neuroradiologists' and general radiologists' in detecting intracranial aneurysms by MRA. Although a number of studies have reported on CAD schemes for the detection of aneurysms, there have been no reports on the detection of lacunar infarcts without our previous study.

The detection of asymptomatic lacunar infarcts in MRIs is also important because their presence indicates an increased risk of severe cerebral infarction (13,14). However, accurate identification of lacunar infarcts on MRIs is difficult for radiologists because of the difficulty in distinguishing the lacunar infarcts from normal tissues such as enlarged Virchow-Robin spaces (15). Therefore we have been developed a CAD scheme for the detection of lacunar infarcts.

In our previous study, Yokoyama et al developed two methods for detection of isolated lacunar infarcts and lacunar infarcts adjacent to a lateral ventricle (2). These methods were applied to 80 cases and the results obtained indicated that the methods were useful in the detection of two different types of lacunar infarcts (3). However, further studies using a larger dataset were necessary for evaluating our computerized method. Therefore in this study, we selected 1,143 T1- and 1,143 T2-weighted images obtained from 132 patients and made a larger database. In addition, we developed a new method for eliminating the false positives (FPs). We determined 12 features by using a new filter bank technique, and then the rule-based schemes and a support vector machine (SVM) with 12 features were employed for distinguishing between the lacunar infarcts and FPs. Furthermore, the detection performance of our improved CAD scheme was evaluated using a larger database.

MATERIALS AND METHODS

Clinical Cases

Our database consisted of 1,143 T1- and 1,143 T2-weighted MR images, which were selected from 132 patients (mean age 63.4 years; age range 28–83 years).

These images were acquired using a 1.5 T magnetic imaging scanner (Signa Excite Twin Speed 1.5 T; GE Medical Systems, Milwaukee, WI) at the Gifu University Hospital (Gifu, Japan). The T1- and T2-weighted images were obtained using the fast spin-echo method with an effective echo time of 8–12 milliseconds, and 96–105 milliseconds, respectively, and a repetition time of 300–500 milliseconds and 3000–3500 milliseconds, respectively. All MRIs were obtained in the axial plane with a section thickness of 5 mm with a 2-mm intersection gap, which covered the whole brain. The matrix size of the MRIs was 512×512 , with a spatial resolution of 0.47 mm/pixel.

Gold Standard

We performed an observer study to determine the location of the lacunar infarcts on the images in our database. On a CRT monitor and using a mouse, two experienced neuroradiologists independently marked the location of the lacunar infarcts (diameter 3–15 mm) on 1,143 T1- and 1,143 T2-weighted MRIs. T1- and T2-weighted images of the same section were displayed together. The slice images for each study were changed manually by the observer. The windowing in T1- and T2-weighted images was initially set to a default value that could be adjusted by the observer. The results revealed that the observer A selected 120 candidates for lacunar infarcts, whereas the observer B selected 154 candidates, implying that accurate identification of lacunar infarcts is difficult.

In this study, a candidate that was identified by both the neuroradiologists was considered as a "lacunar infarct." The sensitivity for the detection of lacunar infarcts was calculated based on the location of the lacunar infarct. On the other hand, the number of FPs per image was calculated based on the "non-lacunar slices." A slice was determined as non-lacunar when a point on the slice was not identified as a lacunar infarct by either of the two neuroradiologists. Our database included 93 lacunar infarcts and 1,063 non-lacunar slices.

Extraction of the Cerebral Region

Lacunar infarcts were generally detected in the basal ganglia region and in the white matter regions. Therefore we first segmented the cerebral region using the region growing technique to avoid detecting false findings located outside the cerebral region. A 3×3 median filter was applied to the T1-weighted image for eliminating impulse noise, and we plotted a histogram of the T1-weighted image thus obtained. All pixels of the brightest

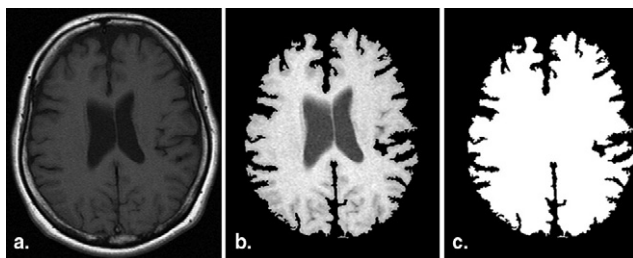


Figure 1. Segmentation of the cerebral region. (a) The original T1-weighted image. (b) Result of the region growing technique. (c) The segmented cerebral region.

peak point in the histogram of the T1-weighted image were used as seed points. The region was then grown by appending to each seed point when the difference between a point of interest and a value in the neighboring pixel was less than 15. Figure 1 illustrates the process adopted for segmentation of the cerebral region. Figures 1a and b show a T1-weighted image and the image obtained on applying the region growing technique, respectively. The small islands were eliminated using size-based feature analysis. Black islands such as the lateral ventricle were filled. The remaining largest white island was determined as the cerebral region. Figure 1c indicates the segmented cerebral region. The search area for the detection of lacunar infarcts was restricted to the segmented cerebral region.

Determination of Initial Candidates for Lacunar Infarcts

The lacunar infarcts were classified into two types based on their location: the isolated lacunar infarct (Fig 2a) and lacunar infarct adjacent to the lateral ventricle (Fig 2b). The former can be easily extracted using a simple thresholding technique. However, it is difficult to extract the latter because the adjacent lateral ventricle will have also a high intensity value and its pixel value will be similar to that of the lacunar infarct. To overcome this issue, we first applied the white top-hat transformation to the T2-weighted images. This procedure enhances white patterns smaller than the structure element used. The structure element was set as a square of 16×16 pixels to enhance the lacunar infarcts while suppressing the normal structures. Figures 2c and d illustrate the images obtained on white top-hat transformation. As shown in these figures, using this method, both the isolated lacunar infarct and the lacunar infarct adjacent to the lateral ventricle were enhanced. Thus extraction of the lacunar infarcts adjacent

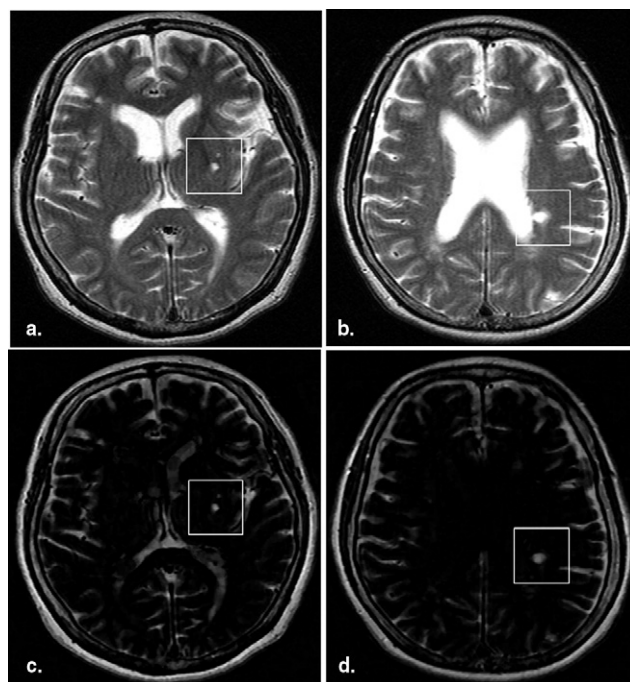


Figure 2. Efficacy of white top-hat transform in the enhancement of lacunar infarcts. (a) T2-weighted image with an isolated lacunar infarct. (b) T2-weighted image with a lacunar infarct adjacent to lateral ventricle. (c) The result image of (a) by using white top-hat transform. (d) The result image of (b) by using white top-hat transform. The white rectangular areas indicate lacunar infarcts.

to the lateral ventricle is rendered easy using a thresholding technique.

By applying a thresholding technique to the image after white top-hat transform, we can determine the initial candidates for lacunar infarcts. However, the pixel values of lacunar infarcts on MRIs change according to the phases, that is, whether acute, subacute, or chronic. Therefore it is difficult to detect the lacunar infarcts by using a fixed threshold value. To solve this problem, we employed multiple-phase binarization. In this procedure, thresholding techniques with several threshold values were applied to the T2-weighted images after white top-hat transformation. In this study, the thresholds for multiple-phase binarization were determined by increasing the pixel value from 55 to 205 at 15-pixel intervals. The total phase number of threshold values was 11. The size and degree of circularity were then calculated in each candidate region in the 11 binarized images. The regions were considered to be candidates for lacunar infarcts when the size was in the range of 33–285 pixels and the degree of circularity was greater than 0.59. The degree of circularity was defined as the fraction of the overlapped area of the candidate with the circle having the same area as the candidate. The ini-

tial candidates for lacunar infarcts were determined by integrating the gravity centers of all candidates detected by multiple-phase binarization. If a candidate center appeared twice or more within a 3×3 square region away from the gravity center of the candidate, it was considered as lacunar infarct candidate. On the other hand, if it appeared only once, it was regarded as FP and was eliminated.

Twelve Features for Elimination of FPs

Using the techniques described in the previous section, most of the lacunar infarcts were detected accurately. However, the candidates selected initially also included many FPs. For eliminating these, we determined 12 features in each initial candidate for a lacunar infarct. These features included the locations x and y , signal intensity differences in the T2- and T1-weighted images, nodular components (NC) from a scale of 1 to 4 in filter bank technique, and nodular and linear components (NLC) from a scale of 1 to 4.

Location.—The locations x and y were defined based on the center of gravity in the candidate regions. Lacunar infarcts occur within cerebral vessel regions. Thus candidates on the periphery of the cerebral region have a strong possibility of being FPs. Based on the location, these candidates could be eliminated as FPs.

Signal intensity difference.—The signal intensity differences in the T1- and T2-weighted images were also important features for distinguishing between lacunar infarcts and FPs. This is because lacunar infarcts show hypointense on T1-weighted images and hyperintense on T2-weighted images. To quantify these characteristics, we determined the signal intensity difference on T1- and T2-weighted images was determined by the difference in the value between the average pixel value of the lacunar infarct region and the average pixel value of the peripheral region. The lacunar infarct region was defined as the region having the maximum area when multiple phase binarization was applied. The peripheral region was defined as the differential regions between the binary image of lacunar infarcts and its expanded regions. The expanded region was calculated by applying the dilation process to the binarized region of the lacunar infarct three times in succession.

NCs and NLCs.—The NC and NLC from a scale of 1 to 4 were calculated using a new filter bank technique (16–18). This filter bank has three important features: 1) it allows the enhancement of the nodular patterns; 2) it allows the enhancement of the nodular and linear patterns; and 3) its sub-

images can be used to reconstruct the original images. For distinguishing between lacunar infarcts and FPs, it may be important to detect both nodular patterns, such as those of the lacunar infarcts, and linear patterns, such as those of a part of the cerebral sulcus. To detect these components, we used the second derivatives. The analysis bank of this filter bank yields the second derivative images in various sizes in the horizontal, vertical, and diagonal directions. The values of the second derivative for the nodular structure in all directions tend to be in the negative. However, the value of the second derivative for the linear structure tends to be zero in the direction of the axis of the linear structure, whereas it tends to be in the negative in the direction perpendicular to the axis of the linear structure. The smallest and largest values of the second derivatives in all directions can be calculated by the smallest eigenvalue and the largest eigenvalue of the Hessian matrix. Thus the NC image was defined based on the absolute value of the largest Eigenvalue of the Hessian matrix. On the other hand, the NLC image was defined based on the absolute value of the smallest Eigenvalue of the Hessian matrix. Figure 3 shows the subimages for NC and NLC both from a scale of 1 to 4, which were obtained from the images for the lacunar infarcts and FPs. As shown in this figure, the small lacunar infarct is enhanced at the small scale. However, the large lacunar infarct is enhanced at the large scale. For determining the NC and NLC, a region of interest with a matrix size of 100×100 was selected at the center of the candidate region. Using the region of interest, we plotted the cumulative histograms of the subimages for the NC and NLC. The NC at each scale from 1 to 4 was determined by the average pixel value higher than 95% of the cumulative histogram of the subimage for nodular patterns at each scale from 1 to 4. The NLC at each scale from 1 to 4 was determined in the same manner by using the subimage for nodular and linear patterns at each scale from 1 to 4.

Elimination of FPs

The rule-based scheme with 12 features was employed as the first step in the elimination of FPs. In this scheme, we first calculated the maximum and minimum values of all lacunar infarcts detected in the initial step for identifying the lacunar candidates. The total 24 cutoff thresholds were then used for eliminating FPs (ie, when a candidate was located outside the range determined by the cutoff thresholds in the feature space, the candidate was considered as FP).

For further elimination of FPs, we employed an SVM (19) with 12 features. SVM is a novel generation learning

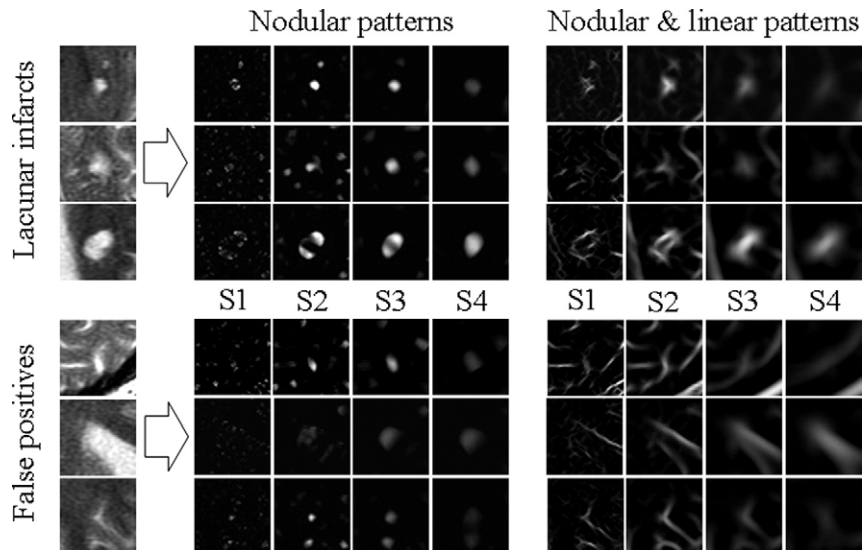


Figure 3. Nodular patterns and nodular and linear patterns from the scale 1 to 4 (S1–S4). These patterns were obtained from the lacunar infarcts and false positives by using the filter bank technique.

system based on recent advances in statistical learning theory. In this article, we considered two kernel types: polynomial and Gaussian kernels. These are among the most commonly used kernel in SVM research. For training and testing the SVM, we used the holdout method (20). In this method, our database was randomly divided into two sets: A and B. The former was first used for training and the latter for testing. This was then reversed (ie, set B was used for training and set A for testing). In this process, we finalized on the following variables: the type of kernel function, its associated parameter, and the regularization parameter C in the structural risk function. To optimize these parameters, we employed an Az value (21). This is the area under the receiver operating characteristic (ROC) curve, and it indicates the accuracy for distinguishing between lacunar infarcts and FPs. In this study, we used the polynomial kernel with the kernel order 1. The parameter C was set at 50. The numbers of input and output unites for SVM were set at 12 and 1, respectively. The output value of the SVM indicates the likelihood of lacunar infarcts. By changing the threshold level of the output, we can determine the performance for detection of lacunar infarcts obtained using our CAD scheme.

RESULTS

To investigate the performance of our CAD scheme, we applied it to the T1- and T2-weighted images in our

database. As the first step toward identifying the initial candidates for lacunar infarcts, 96.8% (90/93) lacunar infarcts were detected accurately with 6.88 (6,771/1,063) FPs per image. This result indicates that a combination of white top-hat transformation and multiple-phase binarization was useful in the detection of lacunar infarcts because most of the lacunar infarcts were detected accurately. However, a problem is that many FPs were also detected together using this method.

For the elimination of FPs, we determined 12 features from each of the initial candidates. Figure 4 shows the mean values and the standard deviations of each of 12 features for the lacunar infarcts and FPs. These features were normalized using all cases in the database. As shown in this figure, the NCs from a scale of 1 to 4 contributed to a great extent in distinguishing between lacunar infarcts and FPs because they showed a greater difference between the mean values for the lacunar infarcts and FPs. Table 1 shows the results of tests for univariate equality of group means. Wilks' lambda (22) is defined as the ratio of within-group variance to the total variance and indicates the degree of discrimination between lacunar infarcts and FPs; for the NC at scale 3, this value was lesser than that for any other feature. The F -value (22) for the NC at scale 3 was also higher than that for any other feature. This result indicates that the NC at scale 3 greatly contributes in distinguishing between lacunar infarcts and FPs. The location features contributed to some extent in eliminating FPs. Additionally, the location fea-

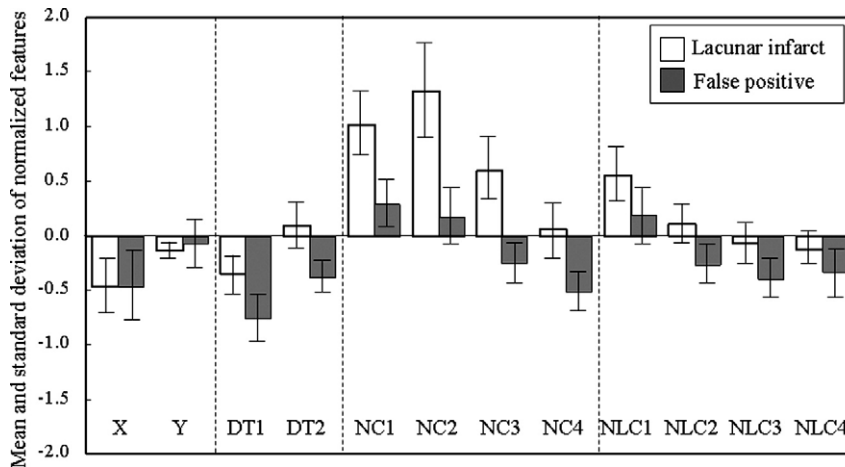


Figure 4. The mean values and the standard deviations of each of 12 features for the lacunar infarcts and false positives. The 12 features consisted of location x (X), location y (Y), signal intensity difference in T1-weighted image (DT1), signal intensity difference in T2-weighted image (DT2), nodular components (NC) from the scale 1 to 4, and nodular and linear component (NLC) from 1 to 4.

Table 1
Test for Univariate Equality of Group Means in Distinguishing Between Lacunar Infarcts and FPs

Feature	Willis's Lambda	F Value	P Value
Location x	1.000	0.003	.954
Location y	0.999	7.534	.006
Density deference T1	0.986	95.372	<.001
Density deference T2	0.955	324.377	<.001
NC at scale 1	0.966	239.583	<.001
NC at scale 2	0.938	456.921	<.001
NC at scale 3	0.934	486.145	<.001
NC at scale 4	0.967	231.115	<.001
NLC at scale 1	0.994	41.351	<.001
NLC at scale 2	0.977	162.121	<.001
NLC at scale 3	0.980	1239.512	<.001
NLC at scale 4	0.996	24.581	<.001

tures were useful in eliminating some FPs on the periphery of the cerebral region. Thus we successfully used the location features as a parameter in this study. To investigate the usefulness of the 12 features, we employed the rule-based scheme with 12 features for eliminating FPs. The results revealed that our CAD scheme achieved the same sensitivity of 96.8% (90/93) with 1.01 (1,071/1,063) FPs per image. Thus 82.8% FPs were eliminated successfully using this scheme. This result indicates that the 12 features were useful in distinguishing between lacunar infarcts and FPs.

For further elimination of FPs, an SVM with the same 12 features was also employed for distinguishing between

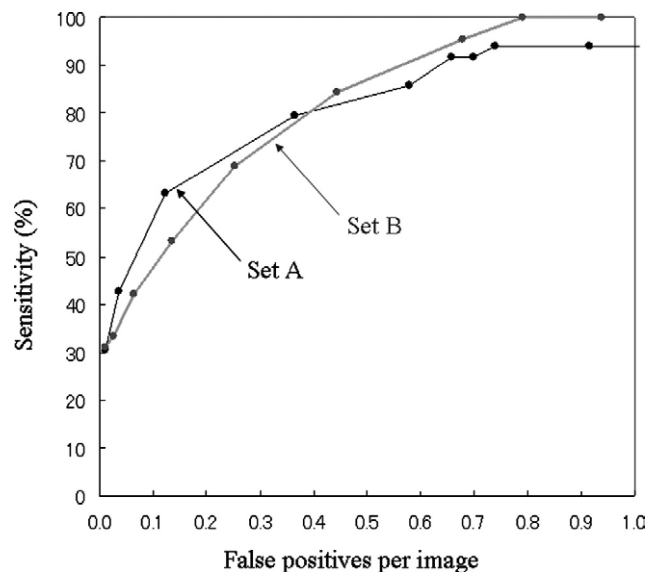


Figure 5. Free-response receiver operating characteristic curves for the overall performance of our computer-aided detection scheme in the detection of lacunar infarcts. For evaluating our method based on holdout method, our database was randomly divided into two sets: set A and set B. The former was first used for training and the latter for testing. This was then reversely (ie, set B was used for training and set A for testing). Two free-response receiver operating characteristic curves represent the results of two sets, respectively.

lacunar infarcts and FPs. Figure 5 shows the free-response ROC curves (23) for the overall performance of our CAD scheme using the SVM with a holdout method as mentioned earlier. These curves were obtained by

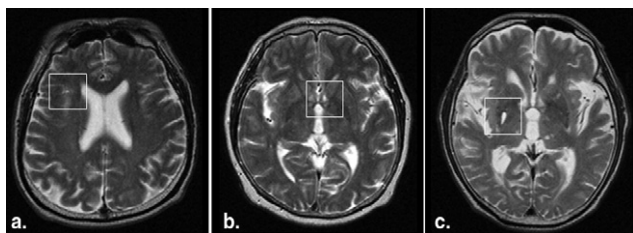


Figure 6. Example of false positives. (a) Part of the cerebral sulcus. (b) Part of the cerebral ventricle. (c) Enlarged perivascular space.

changing the threshold value for the output value of SVM. The result with averaging two curves showed that our CAD scheme achieved the same sensitivity of 96.8% (90/93) with 0.76 (813/1063) FP per image.

DISCUSSION

To investigate the usefulness of CAD schemes, it is imperative to perform an observer study with and without the aid of the CAD output. The results of this study revealed that 96.8% of the lacunar infarcts were accurately detected using our CAD scheme. Therefore the observer's confidence in detecting lacunar infarcts might be increased considering that the outputs of our CAD scheme serve as a "second opinion." On the other hand, there is a possibility of detrimental effect with our CAD scheme. After analyzing 813 FPs obtained using our method, the FPs were classified into four types: a part of the cerebral sulcus, 50.3% (409/813); a part of the cerebral ventricle, 42.8% (348/813); the enlarged perivascular space, 4.1% (33/813); and others, 2.8% (23/813). **Figure 6** shows the examples of each FP type. A part of the cerebral sulcus and a part of the cerebral ventricle can be easily to distinguishing from lacunar infarcts. Thus the detrimental effect would not be occurred using our CAD scheme in these cases. However, an enlarged perivascular space (**Fig 6c**) cannot be easily distinguishing from lacunar infarcts. Therefore an observer might be affected detrimentally by using the output of our CAD scheme.

During the last two decades, many observer studies have been carried out for investigating the usefulness of CAD schemes. For example, these include the detection of microcalcifications on mammograms (24), the distinction between benign and malignant microcalcifications on mammograms (25), the detection of lung nodules on chest radiography (26), the distinction between benign and malignant solitary pulmonary nodules on chest radiography

(27), the detection of lung cancers on CT images (28), and the detection of intracranial aneurysms on MRA images (12). However, to our knowledge, there have been no reports on an observer study on the detection of lacunar infarcts. Therefore to investigate the usefulness of our CAD scheme for the detection of lacunar infarcts in MR images, in the future, it will be necessary to carry out an observer study by using the ROC analysis to compare a radiologist's performance with and without the aid of the CAD output.

Although the sensitivity for detection of lacunar infarcts obtained using our CAD scheme was reported to be 96.8% in this study, the image database used was selected from only one hospital. Therefore the cases might have been influenced by the quality of the linear components scanner and acquisition parameters such as the echo time and repetition time. Thus in the future, we need to expand our database by collecting images from various linear components scanners from several hospitals, and then evaluate our method by using independent databases.

CONCLUSIONS

We have developed a CAD scheme for detection of lacunar infarcts on MRIs. Using this method, the sensitivity for the detection of lacunar infarcts was 96.8% (90/93) with 0.76 FP per image. Therefore our computerized scheme would be useful in assisting radiologists in identifying lacunar infarcts on MRIs.

ACKNOWLEDGMENTS

The authors would like to thank Akiko Kano and Hitoshi Futamura, from Konica Minolta Medical & Graphic, Inc, and Yoshinori Hayashi and Masakatsu Kakogawa, from TAK Co, Ltd, for their valuable suggestions. The authors are also thankful to the staff of Fujita Laboratories, Department of Intelligent Image Information, Graduate School of Medicine, Gifu University, Japan.

REFERENCES

1. Health and Welfare Statistics Association. Vital Stat Jap 2003; 1.
2. Yokoyama R, Lee Y, Hara T, et al. An automated detection of lacunar infarct regions in brain MR images: preliminary study (in Japanese). *Jap J Radiol Tech* 2002; 58:399-405.
3. Yokoyama R, Matsui A, Fujita H, et al. Development of an automated method for detection of lacunar infarct regions on brain MR images. *Proc 19th Int Congress Exhibition CARS 2005. International Conference Series 2005*; 1281:1407.
4. Uchiyama Y, Matsui A, Yokoyama R, et al. CAD scheme for detection of lacunar infarcts in brain MR image. *Int J Comp Assisted Radiol Surg* 2006; 1:382-385.

5. Uchiyama Y, Ando H, Yokoyama R, et al. Computer-aided diagnosis scheme for detection of unruptured intracranial aneurysms in MR angiography. *Proc IEEE Engineering Med Biol 27th Annu Int Conf 2005*; 3031-3034.
6. Uchiyama Y, Yamauchi M, Ando H, et al. Automated classification of cerebral arteries in MRA images and its application to maximum intensity projection. *Proc IEEE Engineering Med Biol 28th Annu Int Conf 2006*; 4865-4868.
7. Yamauchi M, Uchiyama Y, Yokoyama R, et al. Computerized scheme for detection of arterial occlusion in brain MRA images. *Proc SPIE Med Imaging, Computer-Aided Diagnosis*, 6514, 65142C-1-65142C-9, 2007.
8. Arimura H, Li Q, Korogi Y, et al. Automated computerized scheme for detection of unruptured intracranial aneurysms in three-dimensional MRA. *Acad Radiol 2004*; 11:1093-1104.
9. Arimura H, Li Q, Korogi Y, et al. Computerized detection of intracranial aneurysms for three-dimensional MR angiography: feature extraction of small protrusions based on a shape-based difference image technique. *Med Phys 2006*; 33:394-401.
10. Hayashi N, Masutani Y, Matsumoto H, et al. Feasibility of a curvature-based enhanced display system for detection cerebral aneurysms in MR angiography. *Magn Res Med Sci 2003*; 2:29-36.
11. Kobashi S, Kondo K, Hata Y. Computer-aided diagnosis of intracranial aneurysms in MRA images with case-based reasoning. *IEICE Trans Inform Syst 2006*; E89-D(1):340-350.
12. Hirai T, Korogi Y, Arimura H, et al. Intracranial aneurysms at MR angiography: effect of computer-aided diagnosis on radiologists' detection performance. *Radiology 2006*; 237:605-610.
13. Kobayashi S, Okada K, Koide H, et al. Subcortical silent brain infarction as a risk factor for clinical stroke. *Stroke 1997*; 28:1932-1939.
14. Vermeer SE, Hollander M, Dijk EJ, et al. Silent brain infarcts and white matter lesions increase stroke risk in the general population. *The Rotterdam Scan Study. Stroke 2003*; 34:1126-1129.
15. Boukura H, Kobayashi S, Yamaguchi S, et al. Discrimination of silent lacunar infarction from enlarged Virchow-Robin spaces on brain magnetic resonance imaging and pathological study. *J Neurol 1998*; 245: 116-122.
16. Nakayama R, Uchiyama Y. Development of new filter bank for detection of nodular pattern and line patterns in medical images. *Syst Comp Jap 2005*; 36:81-91.
17. Nakayama R, Uchiyama Y, Yamamoto K, et al. Detection of clustered microcalcifications on mammograms using new filter bank. *Syst Comp Jap 2005*; 36:68-79.
18. Nakayama R, Uchiyama Y, Yamamoto K, et al. Computer-aided diagnosis scheme using a filter bank for detection of microcalcification clusters in mammograms. *IEEE Trans Biomed Engineer 2006*; 53:273-283.
19. Cristianini N, Taylor JS. *An introduction to support vector machines and other kernel-based learning methods*. New York: Cambridge University Press, 2000.
20. Theodoridis S, Koutroumbas K. *Pattern recognition*. London: Academic Press, 1999.
21. Metz CE, Herman BA, Shen JH. Maximum likelihood estimation of receiver operating characteristic (ROC) curves from continuously distributed data. *Stat Med 1998*; 17:1033-1053.
22. Johnson RA, Wichern DW. *Applied multivariate statistical analysis*. Prentice Hall, Englewood Cliffs, NJ: 2007.
23. Chakraborty DP. Maximum likelihood analysis of free-response receiver operating characteristic (FROC) data. *Med Phys 1989*; 16:561-568.
24. Chan HP, Doi K, Vyborny CJ, et al. Improvement in radiologists' detection of clustered microcalcifications in mammograms—the potential of computer-aided diagnosis. *Invest Radiol 1990*; 25:1102-1110.
25. Jiang Y, Nishikawa RM, Schmidt RA, et al. Improving breast cancer diagnosis with computer-aided diagnosis. *Acad Radiol 1999*; 6:22-33.
26. Kobayashi T, Xu XW, MacMahon H, et al. Effect of a computer-aided diagnosis scheme on radiologists' performance in detection of lung nodules on radiographs. *Radiology 1996*; 199:843-848.
27. Shiraishi J, Abe H, Engelmann R, et al. Computer-aided diagnosis for distinction between benign and malignant solitary pulmonary nodules in chest radiographs: ROC analysis of radiologists' performance. *Radiology 2003*; 227:469-474.
28. Li F, Arimura H, Suzuki K, et al. Computer-aided detection of peripheral lung cancers missed at CT: ROC analyses without and with localization. *Radiology 2005*; 237:684-690.